A New Method to Simulate the Microwave Effective Snow Grain Size in the Northern Hemisphere Without Using Snow Depth Priors

Jianwei Yang, Lingmei Jiang, *Member, IEEE*, Juha Lemmetyinen, *Member, IEEE*, and Kari Luojus

***Abstract*—The snow water equivalent (SWE) of a snowpack represents the amount of water it contains. SWE retrieval with passive microwave remote sensing techniques is notably affected by snow metamorphism. The effective snow grain size (effGS) described in the GlobSnow methodology can be retrieved over areas where prior snow depth data are available. However, this dependency on the availability of prior knowledge results in increased retrieval uncertainty in areas where such information is unavailable. In this work, we proposed a new method to predict the effGS using a random forest (RF) model. The results indicated that the geographical location, orographic effects, and seasonal characteristics are important for retrieving the effGS, and they are important components of the kriging interpolation of the daily effGS in the GlobSnow methodology, resulting in spatial and temporal autocorrelation phenomena. We assessed the performances of snow depth priors from either station measurements or gridded products in predicting effGS and found that the RF model is promising for effGS prediction even without snow depth priors. The application of spatially independent verification and 10-fold cross-validation (10-CV) techniques revealed that the effGS estimates generally agreed with GlobSnow reference data over Eurasia, with overall unbiased root mean square error (unRMSE) values of 0.15.0.18 mm, but high errors were observed over North America due to terrain variability and heterogeneous forest cover, with overall unRMSE values ranging from 0.22.0.31 mm. Compared to the GlobSnow methodology, the proposed method does not rely on ground-based prior information, and improved computational efficiency can be achieved.**

***Index Terms*—Effective grain size, Global Snow Monitoring for Climate Research (GlobSnow), machine learning, snow depth priors, snow emission model.**

I. Introduction

THE snow water equivalent (SWE) quantitatively describes the amount of water contained in a snowpack. A comprehensive understanding of both the temporal and spatial patterns of the SWE is crucial for numerous studies and applications, including the global water cycle, human needs, ecosystem services, hydropower operation, and natural hazard management [1], [2], [3], [4], [5].

Microwave signals, typically ranging from 10.65 to 89 GHz, are sensitive to snow depth due to the volume scattering of snowpacks; thus, microwave instruments are suitable for providing SWE information [6], [7], [8], [9]. Spaceborne passive microwave remote sensing has provided a long-time series of brightness temperature (Tb) observations from 1978 to the present, and these data are suitable for climatological investigations. The most widely used SWE products rely primarily on empirical or semiempirical retrieval methods and typically involve a hypothetical linear relationship between snow depth and the Tb difference [7], [10], [11], [12], [13], [14], [15]. However, these methods face critical challenges associated with spatiotemporal variations in snow metamorphism, which results in high uncertainty in SWE estimates [16], [17], [18], [19], [20].

Physical-based lookup tables or assimilation methods typically involve the application of large amounts of in situ prior data (e.g., snow depth, grain size, and snow density) to drive the snow forward model and minimize the difference between the modeling values and satellite observations [8], [21], [22], [23], [24], [25], [26], [27], [28]. Therefore, these algorithms can reduce the errors caused by snow microstructure variations and provide more reliable SWE estimates than can empirical or semiempirical methods. However, the lack of spatially distributed and temporally continuous grain size priors restricts their application at the global scale.

The SWE retrieval approach of Global Snow Monitoring for Climate Research (GlobSnow) entails the utilization of the effective snow grain size (effGS) to constrain the snow microwave emission model for improving SWE estimates [8], [22]. The effGS, a variable that effectively characterizes the seasonal evolution of grain size, can be optimized through the snow forward model by minimizing the difference between satellite observations and snow emission model simulations. First, a snow forward model, namely, the Helsinki University of Technology (HUT) model, can be used to optimize the effGS by minimizing the difference between the modeling output and the observed Tb at the weather station scale and then extending the effGS over the entire area of interest by kriging interpolation. Finally, SWE estimates can be obtained through Bayesian nonlinear

Manuscript received 3 January 2024; revised 29 March 2024 and 29 May 2024; accepted 25 July 2024. Date of publication 12 August 2024; date of current version 5 September 2024. This work was supported in part by the National Natural Science Foundation of China under Grant 42090014 and Grant 42201346 and in part by the Fundamental Research Funds for the Central Universities under Grant 2021NTST02. *(Corresponding author: Lingmei Jiang.)*

Jianwei Yang and Lingmei Jiang are with the Faculty of Geographical Science, Beijing Normal University, Beijing 100875, China (e-mail: yangjw@bnu.edu.cn; jiang@bnu.edu.cn).

Juha Lemmetyinen and Kari Luojus are with the Finnish Meteorological Institute, 00101 Helsinki, Finland (e-mail: juha.lemmetyinen@fmi.fi; kari.luojus@fmi.fi).

Digital Object Identifier 10.1109/JSTARS.2024.3441817

assimilation by leveraging the effGS outputs and snow depth priors obtained via kriging interpolation [22].

Although GlobSnow provides more reliable global SWE estimates than other remote sensing products in the Northern Hemisphere [29], [30], [31], snowpack monitoring remains challenging due to its low computational efficiency and high complexity of implementation, e.g., spatial interpolation, error calculation, and iterative assimilation. Moreover, synoptic weather station measurements are applied in the form of a prior field to optimize effGS in the HUT model. The representativeness of weather stations for satellite pixels is unknown or problematic because of the large disparity in resolution between point measurements and coarse satellite pixels (the so-called scale effect) [32]. In addition, the dependence on snow depth priors partially delays the real-time or near-real-time monitoring of the SWE.

The purpose of this work was to establish a new method for predicting the effGS without using ground-based snow depth observations. Numerous studies have indicated that machine learning-based algorithms, e.g., random forest (RF), convolutional neural networks (CNN), and support vector machine (SVM), exhibit high potential for snow depth retrieval [26], [33], [34], [35], [36], [37], [38], [39]. However, their potential for simulating grain size has not been fully explored.

Our main objectives were to (1) explore, for the first time, the possibility of predicting the effGS using the RF model, (2) demonstrate whether snow depth priors contribute to improving effGS retrieval, and (3) verify RF model estimates and compare them to GlobSnow effGS data in the Northern Hemisphere.

The rest of this article is organized as follows. In Section II, the data and methodology are provided. The obtained results are illustrated in Section III. In Section IV, algorithm-related sources of uncertainty are examined. Finally, in Section V, conclusions are outlined, and further applications of the proposed method are described.

II. Data and Methodology

A. Ground-Based Snow Depth Measurements

To test the role of snow depth priors in retrieving effective grain size, ground-based snow depth measurements were used in this study. The Global Historical Climatology Network-daily (GHCN-Daily) snow depth dataset was obtained from http://www.ncdc.noaa.gov/oa/climate/ghcn-daily/ [Fig. 1(a), black points]. Due to the limited spatial coverage of the GHCN-Daily dataset across China, many Chinese station measurements acquired from the China Meteorological Data Service Center (http://data.cma.cn/en) were supplemented herein [Fig. 1(a), gray points]. Daily snow depth measurements from these stations over the 2012–2018 period were used. In this study, only snow depth values obtained under dry conditions (an air temperature below zero) were selected as training samples.

To demonstrate the feasibility of retrieving the effGS using the RF model, numerous spatially independent sites were selected. Fig. 1(b) shows the spatial distribution of the validation stations (red points) in the Northern Hemisphere. The site locations in Eurasia were determined by snow course data available at http://meteo.ru/english/data/. The automatic observation station locations in North America were acquired from the Canadian historical SWE dataset (https://doi.org/10.18164/cf337b6b-9a87-4ffd-a8e5-41e6498b1474). The selected site locations exhibit no spatial overlap with the training stations shown in Fig. 1(a). Thus, the GlobSnow effGS records at these locations can be used as a spatially independent validation dataset for verifying the RF model.

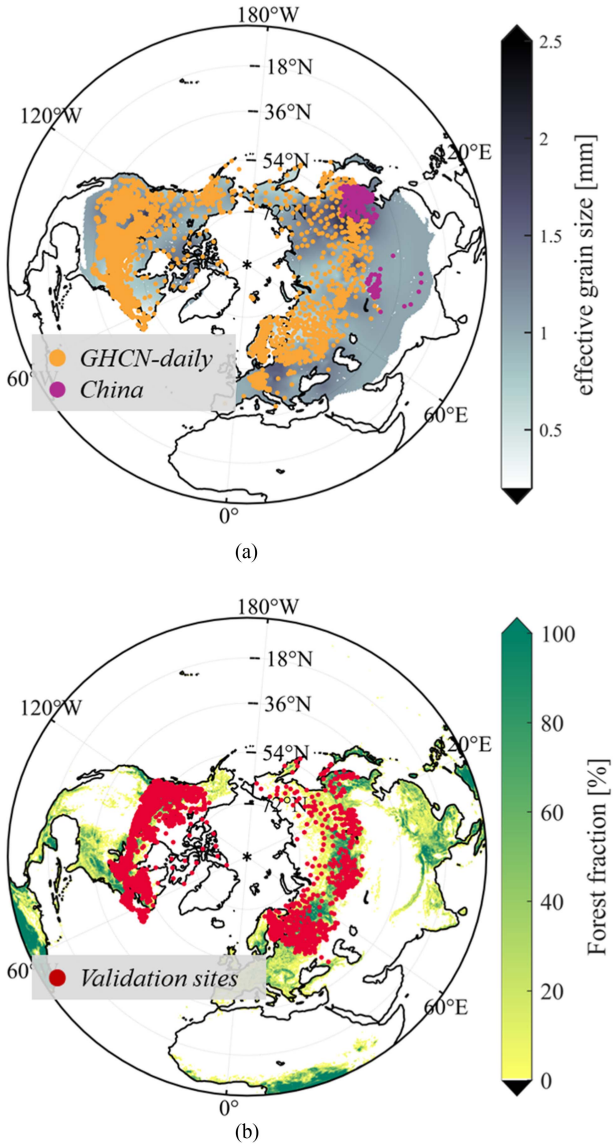

Fig. 1. Distribution of the stations used for (a) RF model training and (b) verification. The GlobSnow effective grain size is shown in the background of (a). The forest fraction is shown in the background of (b).

Moreover, the well-known k-fold cross-validation (k-CV) technique was employed to comprehensively evaluate the performance of the trained RF models in predicting effGS. The methodology and results are described in Sections II-C and III-D, respectively.

B. Gridded Products

The aim of our effGS study was to estimate the SWE at a coarse spatial resolution (~25 km). Therefore, gridded satellite observations were selected. The gridded products used in this study included remotely sensed brightness temperature observations, the GlobSnow-v3.0 effGS product, and the reanalysis ERA5-Land dataset. The Advanced Microwave Scanning Radiometer 2 (AMSR2) Level 3 brightness temperature product is available at http://gportal.jaxa.jp/gpr/since 2012. In this study, the AMSR2 sensor was selected because 10.65 GHz frequency data are available, which facilitates the assessment of the effects of low frequencies in effGS retrieval.

In this study, the GlobSnow-v3.0 effGS product downloaded from www.globsnow.info was regarded as the baseline reference dataset [40]. The methodology is introduced in Section II-C. To demonstrate the role of snow depth in predicting the effGS, the ground-based snow depth was selected. Given the representativeness and accessibility of ground-based snow depth data, we explored the possibility of replacing station-based measurements with gridded products to generate an effGS dataset via the RF approach. Gridded products provide spatially distributed snow depth data, which may be better than interpolated fields from weather station measurements. In this study, the hourly ERA5-land product of the European Centre for Medium-Range Weather Forecasts (https://cds.climate.copernicus.eu/) was chosen because it has been demonstrated that this product outperforms other reanalysis or remote sensing products [30], [41]. The ERA5-land product (0.1° × 0.1°) at 8:00 a.m. was applied because this time point approximately coincides with the station measurement time. To maintain the same spatial resolution, all the gridded products were resampled to the AMSR2 grid. Fig. 2 shows the spatial distributions of the GlobSnow-v3.0 and ERA5-land snow depth data in the Northern Hemisphere. Here, the ERA5-land product was selected due to its sensitivity to deep snow relative to the GlobSnow-v3.0 product. Please refer to the details provided in Section III-A.

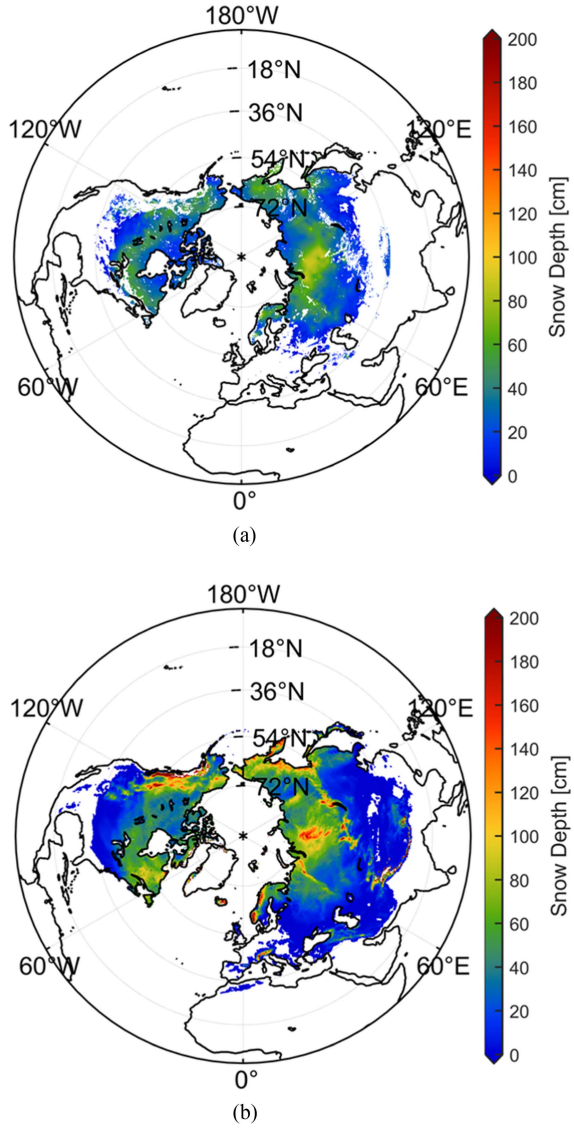

Fig. 2. Spatial distributions of (a) GlobSnow-v3.0 and (d) ERA5-land snow depth data in January 2014 (example).

C. Methodology

The effGS can be optimized utilizing the snow forward model by minimizing the difference between satellite observations and snow emission model simulations at vertically polarized frequencies of 18.7 and 36.5 GHz [17]. The fitting expression is as follows:

$$\begin{aligned}\min_{d0}\{&[\mathrm{Tb}_{18.7\mathrm{V,HUT}}(\mathrm{SD}_{ini},\ \mathrm{d0})\\&-\mathrm{Tb}_{36.5\mathrm{V,\ HUT}}(\mathrm{SD}_{ini},\ \mathrm{d0})]\\&-[\mathrm{Tb}_{18.7\mathrm{V,\ satellite}}-\mathrm{Tb}_{36.5\mathrm{V,\ satellite}}]\}^2\end{aligned}\quad(1)$$

where $\mathrm{Tb}_{18.7\mathrm{V,HUT}}$ and $\mathrm{Tb}_{36.5\mathrm{V,HUT}}$ denote the simulated brightness temperatures of the HUT model at vertically polarized frequencies of 18.7 and 36.5 GHz, respectively; $\mathrm{Tb}_{18.7\mathrm{V,satellite}}$ and $\mathrm{Tb}_{36.5\mathrm{V,satellite}}$ denote satellite-observed brightness temperatures; and $\mathrm{SD}_{\mathrm{ini}}$ denotes the ground-based snow depth, as the background field.

In this study, the RF model was chosen as the machine learning algorithm to explore the nonlinear relationships between multiple independent variables and the effGS due to the favorable performance of this approach in SWE estimation [26], [34], [35]. The values of two key parameters of the RF model, namely, the number of decision trees (*ntree*) in the ensemble and the number of predictor variables (*mtry*) randomly selected at each node, were set to 500 and 4, respectively.

A flowchart of the effGS prediction process through the RF model is shown in Fig. 3. In summary, the first step is to select relevant predictor variables to train the RF model (for details, please refer to Section III-A). Here, to evaluate the role of snow depth in predicting the effGS, both station-based measurements (from the stations shown in Fig. 1) and the spatially continuous reanalysis ERA5-land product were used in RF training (Fig. 3). Here, the ERA5-land product was adopted as a candidate because its overall performance is comparable to that of the GlobSnow-v3.0 product. Moreover, ERA5-derived estimates can reflect deep snowpack conditions. The RF model

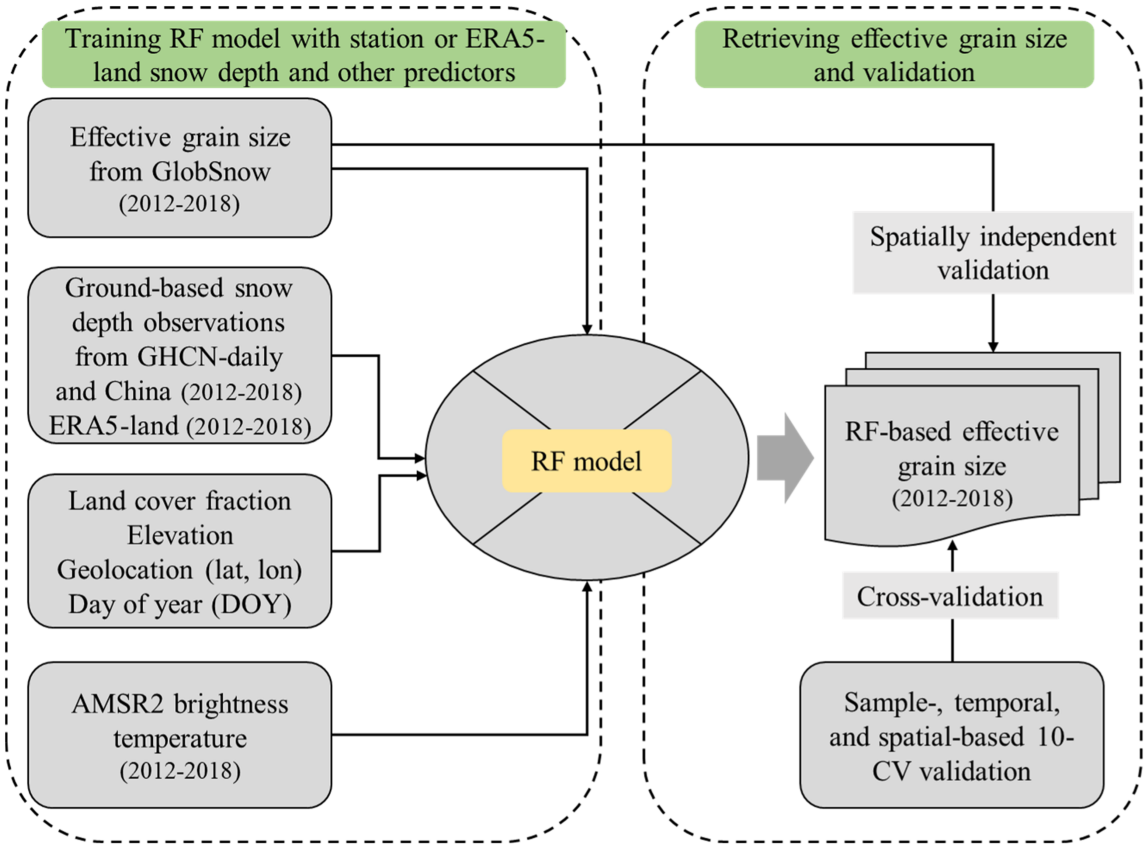

Fig. 3. Flowchart for predicting the effective grain size with the RF model.

was trained to generate effGS time-series datasets from 2012 to 2018. Finally, the RF model estimates were verified against spatially independent GlobSnow effGS reference data [refer to the stations shown in Fig. 1(b)].

Additionally, various well-known k-CV methods, e.g., sample-, time-, and space-independent k-CV techniques [42], [26], were employed to comprehensively assess the ability of the RF model to predict the effGS. First, we randomly divided the sample data into 10 (k = 10) equal subsamples. Then, 9 randomly selected subsamples were used to train the RF model, and the remaining subsample was adopted for assessing the trained RF model. To analyze all samples and avoid overfitting, this procedure was repeated 10 times. Temporal and spatial 10-CV methods were used to assess the performance of the well-trained RF algorithm at temporal and spatial scales. The implementation is similar to that of the sample-based 10-CV method mentioned earlier. The dates (time) and weather stations (space) were randomly divided into 10 equal groups. Generally, the sample-based 10-CV method can capture the training performance, while the temporal and spatial 10-CV methods can represent the temporal and spatial transferability levels, respectively, of the RF models.

To demonstrate whether snow depth priors are helpful for retrieving the effGS, two contrasting algorithms were investigated:

$$RF_{withSD} = f\,(\text{longitude},\ \text{DOY},\ \text{elevation},\text{latitude},\ \mathrm{Tb}_{10.65\mathrm{V}},\mathrm{Tb}_{18.7\mathrm{V}},\mathrm{Tb}_{36.5\mathrm{V}},\mathrm{Tb}_{89\mathrm{V}},\ \text{SD}) \quad (2)$$

$$RF_{withoutSD} = f\,(\text{longitude},\ \text{DOY},\ \text{elevation},\text{latitude},\ \mathrm{Tb}_{10.65\mathrm{V}},\mathrm{Tb}_{18.7\mathrm{V}},\mathrm{Tb}_{36.5\mathrm{V}},\mathrm{Tb}_{89\mathrm{V}}) \quad (3)$$

where SD is the snow depth measured at a weather station or from the gridded ERA5-land product; DOY denotes the day of the year, which ranges from 1 to 365 or 366; and $\mathrm{RF}_{\mathrm{withSD}}$ and $\mathrm{RF}_{\mathrm{withoutSD}}$ denote two well-trained RF models. Regarding the $\mathrm{RF}_{\mathrm{withSD}}$ algorithm, snow depth priors are involved, while no snow depth is used in the $\mathrm{RF}_{\mathrm{withoutSD}}$ algorithm. Notably, $\mathrm{Tb}_{10.65\mathrm{V}}$, $\mathrm{Tb}_{18.7\mathrm{V}}$, $\mathrm{Tb}_{36.5\mathrm{V}}$, and $\mathrm{Tb}_{89\mathrm{V}}$ are observed at vertically polarized frequencies of 10.65, 18.7, 36.5, and 89 GHz, respectively. Here, vertical polarization was considered because its penetration into the forest canopy is greater than that of horizontal polarization [22], [43].

III. Results

A. Selection of the Predictor Variables for the RF Model

To determine the optimal predictor variables for the RF model, the correlation matrix of all possible variables and their importance rankings was obtained, as shown in Fig. 4. The correlation matrix denotes the correlation coefficients among all predictor variables. The importance rankings reflect the relative contributions of the input variables and can be obtained by averaging the difference in the out-of-bag estimation error before and after the permutation of overall decision trees in the RF model. According to the rankings, the nine most important predictors, including

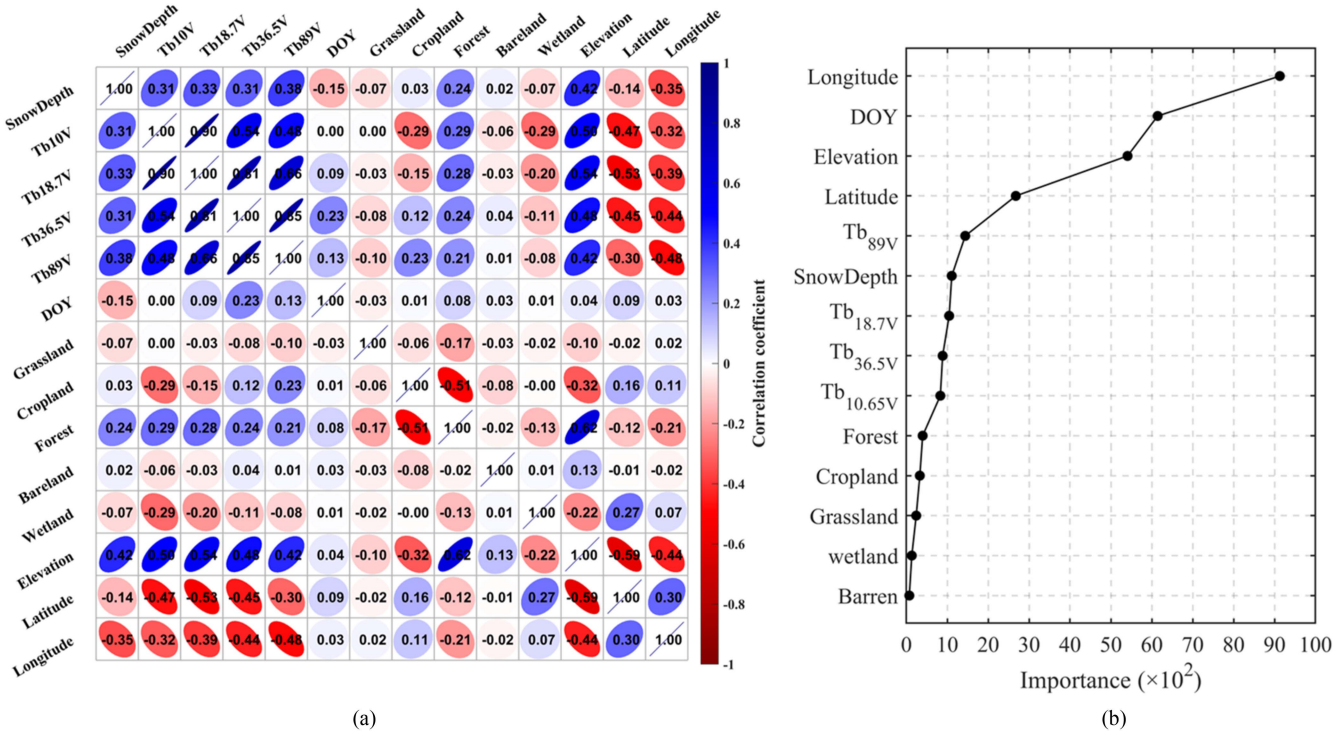

(a) (b)

Fig. 4. (a) Correlation matrix of the selected variables and (b) their importance rankings in predicting the effGS according to the dataset for the 2012–2018 period.

longitude, DOY, elevation, latitude, snow depth, vertically polarized brightness temperature from 10.65 to 89 GHz, etc., were selected for RF model training [Fig. 4(b)]. Longitude, DOY, elevation, and latitude are auxiliary geographical location or terrain parameters and are referred to as static variables. $Tb_{10.65V}$, $Tb_{18.7V}$, $Tb_{36.5V}$, and Tb_{89V} are dynamic variables with data provided by the AMSR2 sensor. Here, only vertical polarization was selected due to its high penetration into the forest canopy relative to horizontal polarization [42]. Moreover, the effGS was optimized with the snow forward model by minimizing the difference between satellite observations and snow emission model simulations under vertical polarization [22]. Fig. 4(a) shows that the satellite-observed brightness temperatures are correlated with the elevation (0.42 to 0.56), longitude (−0.32 to −0.48), and latitude (−0.30 to −0.47), and the dependence of the effGS on the brightness temperature is low. Moreover, brightness temperatures are influenced not only by snow characteristics but also by mixed land cover types, atmospheric conditions, forest cover, and terrain conditions [9]. Therefore, the signals at these four frequencies (10.65–89 GHz) exhibited a weak relationship with the effGS [Fig. 4(b)]. The forest fraction was significantly correlated with elevation, with a correlation coefficient of 0.62 [Fig. 4(a)], which reduced the importance of forest cover for the effGS. The results in Fig. 4(a) indicate that there was a high correlation (−0.59) between latitude and elevation. Longitude exhibited greater importance than latitude in this study [Fig. 4(b)]. This could occur because the longitude ranges from −180 to 180°E in snow-covered areas, while the latitude only ranges from 30°N to 75°N. Moreover, the effGS significantly varied with longitude relative to latitude over the Northern Hemisphere. The correlation matrix explains the importance of ranking in predicting the effGS. The low rankings of some variables do not indicate that they are not important for effGS prediction. Notably, another predictor variable likely plays an alternative role due to the autocorrelation among the various variables. Scatter plots between the predictor variables and effGS are provided in Section III-B.

Fig. 5 shows the validation and comparison of the GlobSnow-v3.0 and ERA5-land products in the Northern Hemisphere. Overall, the two products displayed similar performance levels, with unbiased root mean square error (unRMSE) values of 18.26 and 18.18 cm, respectively. However, the ERA5-land product was more sensitive to greater depths than the GlobSnow-v3.0 product, especially for snowpacks thicker than 60 cm. Therefore, in this study, we selected the ERA5-land dataset as a candidate for evaluating the role of spatially continuous snow depth in predicting the effGS via the RF model. Notably, the bias of the ERA5-Land product was greater than that of the GlobSnow-v3.0 product (0.16 versus 8.60 cm). The errors in effGS prediction caused by snow depth priors were examined. The details are provided in Section IV-C.

B. Relationships Between the GlobSnow Effective Grain Size and Predictor Variables

Scatter plots between the predictor variables and effGS are shown in Fig. 6. The figure shows a nonlinear trend between the effGS and station-based snow depth, first decreasing for snow depths from 0 to 60 cm, then slightly increasing from 60 to 120 cm, and finally stabilizing from 120 to 200 cm [Fig. 6(a)].

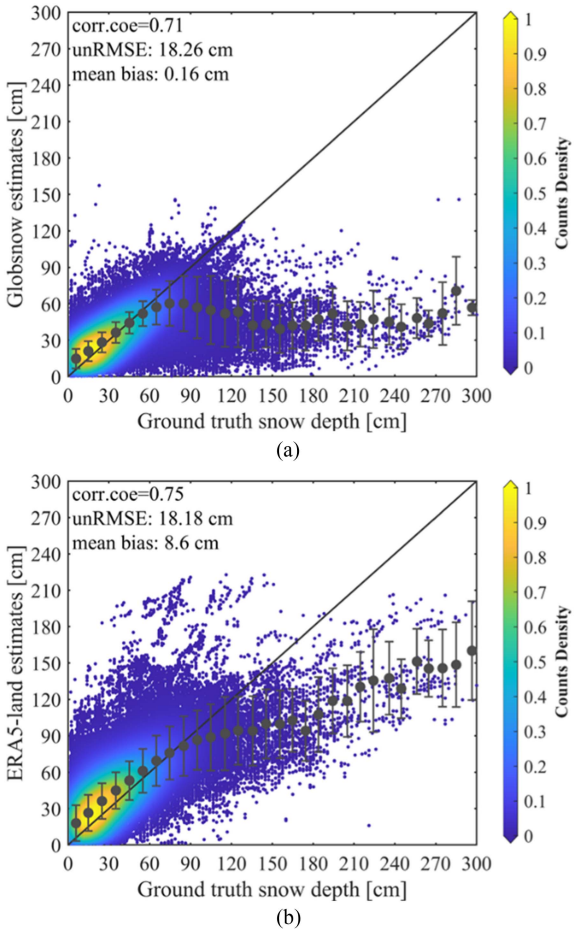

Fig. 5. Validation of (a) GlobSnow-v3.0 and (b) ERA5-land snow depth products in the Northern Hemisphere over the 2012–2018 period.

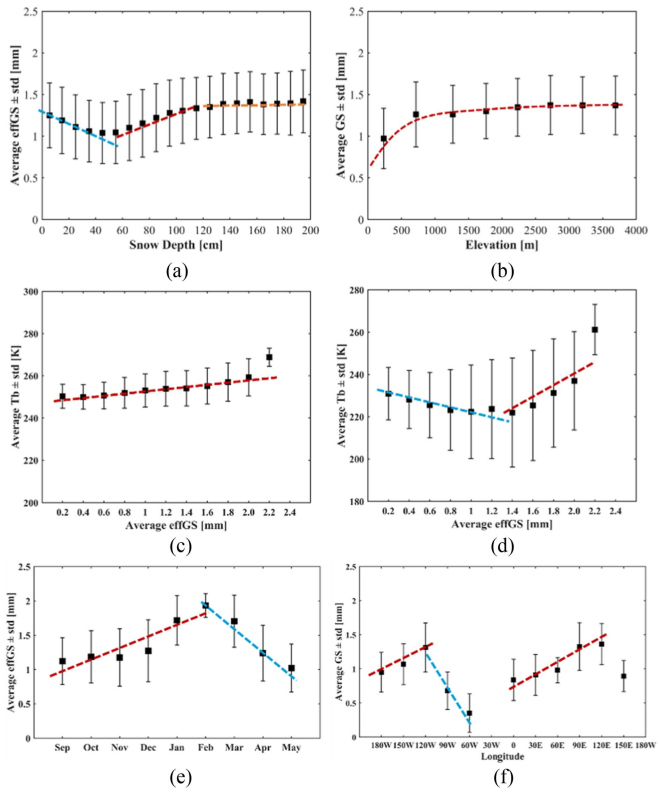

Fig. 6. Statistical relationships between GlobSnow effGS and (a) station-based snow depth, (b) elevation, (c) $Tb_{18.7\ V}$, (d) Tb_{89V}, (e) DOY, and (f) longitude.

Fig. 6(b) shows the logarithmic relationship between the elevation and effGS. The effGS is insensitive to elevations above 1000 m, which indicates that elevation primarily contributes to predicting the effGS in low-elevation areas. Fig. 6(c) and (d) show the relationships between effGS and $Tb_{18.7}$ and Tb_{89} as examples (those for $Tb_{10.65}$ and $Tb_{36.5}$ are not shown). The response of the microwave signal to the effGS is low; for example, a slight upward trend occurs at 18.7 GHz with increasing effGS, while at 89 GHz, a decreasing trend occurs before 1.4 mm, followed by an increasing trend. Although the 89 GHz signal is more sensitive to the effGS than the 18.7 GHz signal is, it exhibits greater uncertainties [refer to the error bar in Fig. 6(d)]. This occurs because signals with high frequencies are sensitive to surface snow and influenced by atmospheric conditions and forest cover [12].

Fig. 6(e) shows the seasonal evolution of the effGS, which increases from September to February of the following year and decreases thereafter. This occurs because single-layer snow is considered in the HUT model to optimize the effGS. The average effGS decreases with increasing snow accumulation. The relationship between effGS and longitude is shown in Fig. 6(f). The changes in effGS with longitude are relatively complex, displaying subsection characteristics. For example, the effGS increases with increasing longitude across Eurasia (0–120°E). In western North America (120–180°W), the relationship is positive, while it is negative in the eastern part (0–120°W). Elevation and longitude are positively correlated with the spatial distribution of snow cover, and the DOY reflects the temporal evolution of the effGS. Thus, these three parameters are the most important predictor variables [Fig. 4(b)].

C. *Effective Grain Size Predicted With the RF Model*

To demonstrate the role of snow depth priors in predicting the effGS with the RF model, a snow forward model, namely, the HUT model, was first used to generate a theoretical database, where the input snow depth ranged from 0 to 200 cm, with steps of 2 cm, and the grain size ranged from 0.1 to 2.8 mm, with steps of 0.05 mm. Then, a comparative experiment based on the theoretical database was conducted to assess the role of snow depth in predicting the effGS. Fig. 7 shows a comparison of the two trained RF models. Fig. 7(a) shows the performance of the trained RF model for snow depth, while snow depth is not included in Fig. 7(b). The results demonstrate that snow depth priors can partially enhance RF model performance, but this effect is not notable; for example, the overall unRMSE decreases from 0.09 to 0.04 mm [Fig. 7(a) versus (b)].

We further employed station-based and ERA5-land datasets (867234 samples) to determine the role of snow depth priors in predicting the effGS (Figs. 8 and 9). Two-thirds of all samples were randomly selected to train the RF model, and the remaining

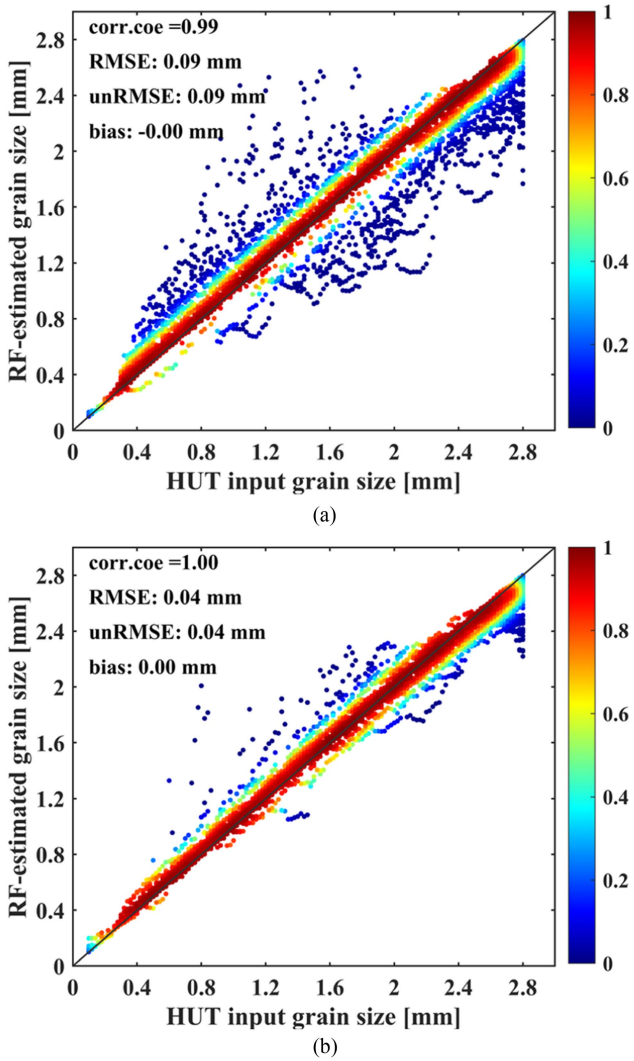

Fig. 7. Density scatterplots of the grain size (artificially defined for the HUT model) and estimates of the RF model trained with (a) HUT-simulated brightness temperature only and (b) HUT-simulated brightness temperature and the defined snow depth. The HUT simulations involve vertical polarization brightness temperatures ranging from 10.65 to 89 GHz.

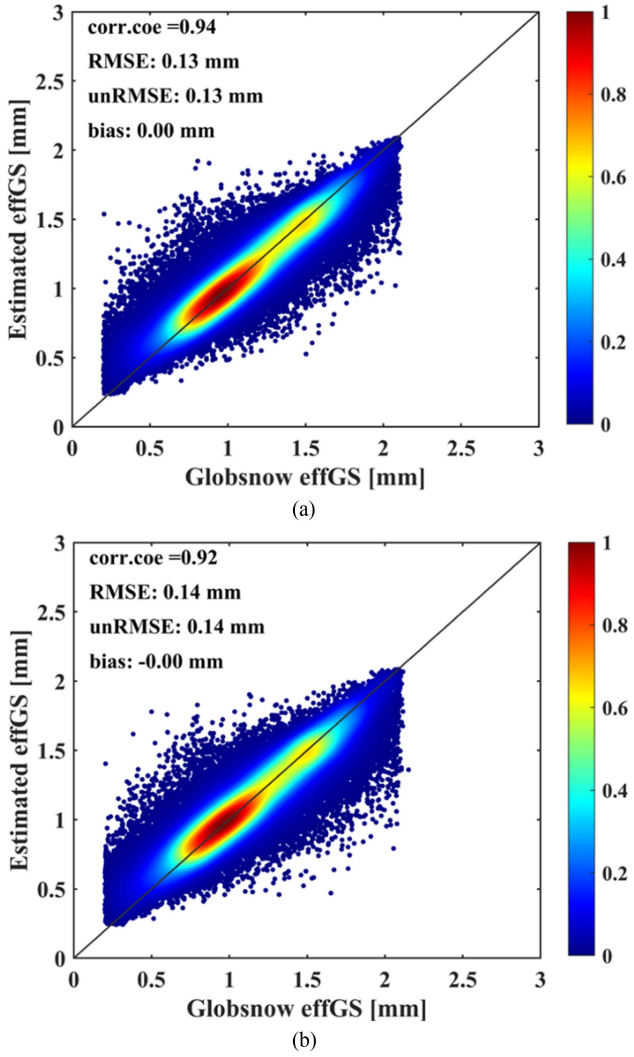

Fig. 8. Comparison of the two well-trained RF models (a) with and (b) without ERA5-land snow depth priors.

samples were used to evaluate its performance. Fig. 8(a) and (b) show scatter plots of the effGS estimates obtained with two trained RF models (Section II-C) with and without the ERA5-derived snow depth values, respectively. Fig. 9(a) and (b) show scatter plots of the effGS estimates obtained with the two trained RF models with and without station-based snow depth values, respectively. Overall, neither the ERA5-land product nor the station snow depth priors enhanced the performance of the RF model for predicting the effGS; for example, the unRMSE values were 0.13 versus 0.14 mm [Fig. 8(a) and (b)] and 0.12 versus 0.13 mm [Fig. 9(a) and (b)], respectively. Moreover, the effGS estimates involving either station-derived or ERA5-derived priors were qualitatively similar [Figs. 8(a) versus 9(a)].

Fig. 10 shows the performance of the trained RF models over various depth ranges. RF_{withSD} and $RF_{withoutSD}$ exhibited similar trends at depths less than 140 cm [Fig. 10(a)]. At depths greater than 140 cm, RF_{withSD} performed better than $RF_{withoutSD}$; for example, the maximum unRMSE values were 0.25 and 0.28 mm, respectively. Fig. 10(b) shows that the overall biases were low. Fig. 11 shows the performance of the RF models at the monthly scale. The overall accuracies of RF_{withSD} and $RF_{withoutSD}$ were similar, but their monthly performance levels differed slightly. The effGS estimates in winter (January, February, March, and December) were closest to the reference values, with unRMSE (coefficient) values of 0.15–0.20 mm (0.85–0.92) and 0.16–0.21 mm (0.85–0.92) for the RF_{withSD} and $RF_{withoutSD}$ models, respectively. This was partially due to stable snow metamorphism during these four months. Fig. 11 shows that $RF_{withoutSD}$ also possibly outperformed RF_{withSD}; for example, in December, the unRMSE values were 0.19 and 0.17, respectively, and the correlation coefficients were 0.85 and 0.88, respectively. The influence of effGS errors on snow depth estimation is described in Section IV-D.

Fig. 12 shows the daily mean time-series effGS values in Eurasia and North America. The black solid dots denote the

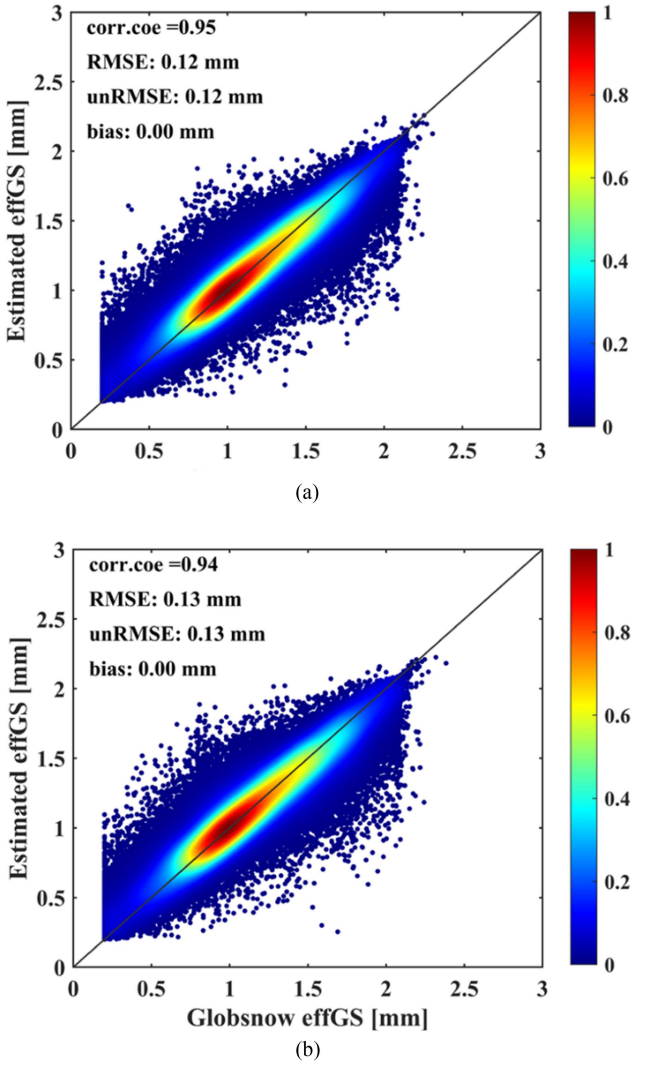

Fig. 9. Comparison of the two well-trained RF models (a) with and (b) without station-based snow depth priors.

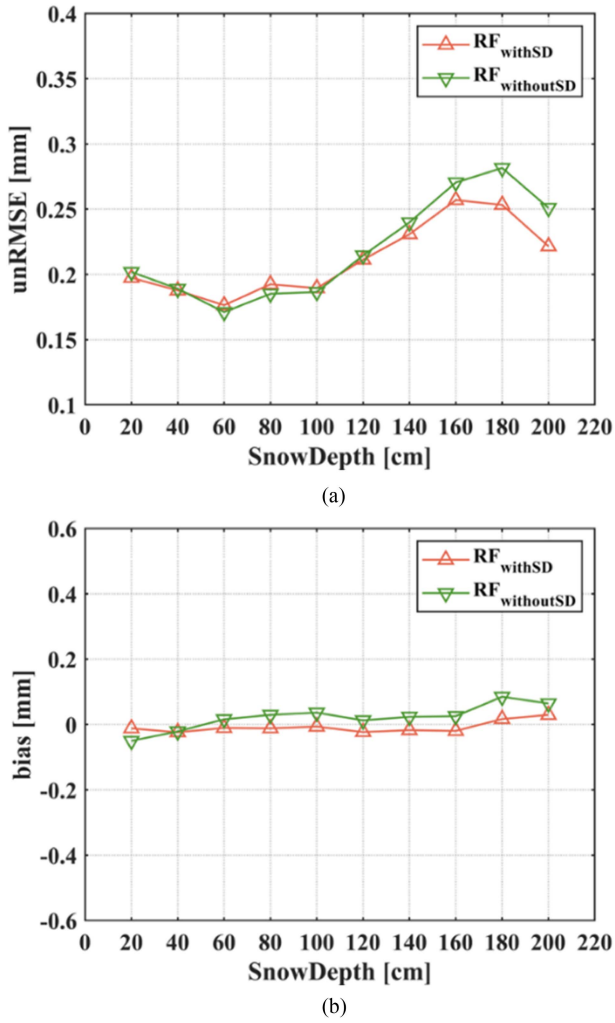

Fig. 10. Performance of the trained RF models at various snow depths.

GlobSnow-v3.0 effGS reference data. The cyan and purple solid dots denote the RF_{withSD} and $RF_{withoutSD}$ effGS estimates, respectively. Overall, the daily average estimates of both RF_{withSD} and $RF_{withoutSD}$ conformed with the GlobSnow reference data, indicating that the effGS estimates are weakly dependent on snow depth overall, similar to the results in Figs. 8–11.

D. Validation and Comparison of the Predicted Effective Grain Sizes

To demonstrate the predictive power of the RF_{withSD} and $RF_{withoutSD}$ models [refer to (2) and (3), respectively], spatially independent datasets from 2012 and 2018 were selected for this study [refer to the stations in Fig. 1(b)]. According to the results in Section III-C, the RF_{withSD} models trained with station-based and ERA5-land snow depth priors exhibited similar performance levels; thus, only snow depth priors from weather stations were used for RF_{withSD} as a case study herein. Fig. 13 shows the validation results over Eurasia. The RF_{withSD} and $RF_{withoutSD}$ models exhibited similar performance levels, for example, with unRMSE (correlation) values of 0.15 (0.93) and 0.16 mm (0.92), respectively. The histogram of errors also shows that 90% of the residual errors between the reference and estimated values were within the [−0.2, 0.2] range [Fig. 13(b)].

Fig. 14 shows the validation results of the RF models in North America. The RF_{withSD} and $RF_{withoutSD}$ models exhibited similar performance levels in terms of unRMSE and correlation values. This further demonstrated that snow depth priors do not notably enhance the predictive power of the RF model. The histogram of residual error shows that 90% of the biases of the reference data and estimates remained within the [−0.3, 0.3] range. Owing to the complex terrain in North America (e.g., the Canadian Rocky Mountains, coastal mountains, San Juan Mountains, and the Appalachian Mountains), the uncertainties in the effGS estimates are greater than those in Eurasia; for example, the unRMSE (correlation) values are 0.15 (0.93) and 0.22 mm (0.81) (Figs. 13 versus 14). A detailed discussion is given in Section IV-A.

Here, we applied the 10-CV method to evaluate the performance of the trained RF models. Due to the similar performance

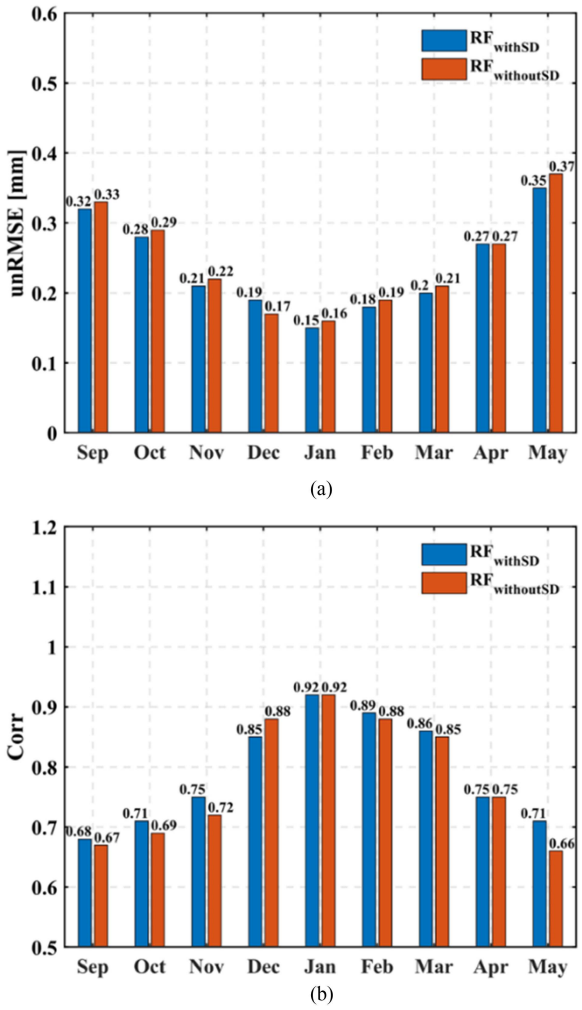

Fig. 11. Monthly performance of the trained RF models in terms of (a) unRMSE and (b) correlation coefficient (corr).

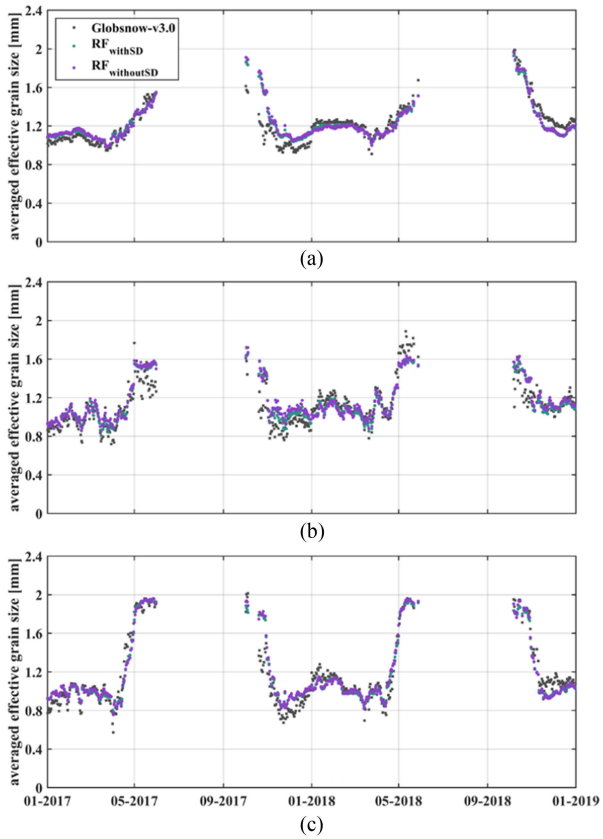

Fig. 12. Time series of the predicted and GlobSnow effGS values from 2017 to 2018 in (a) Eurasia (0–150°E), (b) eastern North America (0–120°W), and (c) western North America (120–180°W).

levels of the RFwithSD and RFwithoutSD models, only the results of RFwithSD are shown as an example. Fig. 15 shows the sample-, temporal-, and spatial-based 10-CV validation results over Eurasia. The overall unRMSE values were 0.10, 0.15, and 0.18 mm for the sample-, temporal- and spatial-based 10-CV methods, respectively. The RFwithSD models performed better temporally than spatially, with unRMSE values of 0.15 and 0.18 mm, respectively. Overall, the effGS estimates agreed with the reference data much better at the sample-, temporal-, and spatial-based scales, which is consistent with the results shown in Fig. 13. Thus, the temporal and spatial transferability levels of the RF model over Eurasia are high.

However, the performance levels of the RFwithSD models over North America at the sample-, temporal-, and spatial-based scales differed (Fig. 16). The overall unRMSE (bias) values were 0.15 (0.00) mm, 0.28 (−0.13) mm, and 0.31 (−0.14) mm for the sample-, temporal-, and spatial-based 10-CV methods, respectively. The unRMSE (bias) values increased from 0.15 (0.00) mm for the sample-based method to 0.31 (−0.14) mm for the spatial-based method, suggesting that in terms of the temporal and spatial transferability levels, the robustness of the RF model over North America is lower than that over Eurasia. A discussion is provided in Section IV-C.

Due to the similar spatial patterns of the RF_{withSD} and $RF_{withoutSD}$ effGS estimates, Fig. 17 only shows the spatial distributions of the RF_{withSD} estimates during the snowy winter season and a comparison with the GlobSnow effGS reference data in the Northern Hemisphere. The spatial patterns of the RF model estimates (first row) and GlobSnow product (second row) are relatively similar during the snowy winter season, indicating that the RF model is reliable for predicting the effGS. The third row in Fig. 17 shows the differences between the RF model estimates and the GlobSnow effGS reference data. The differences in most areas are small, ranging from approximately −0.2 to 0.2 mm. In western Europe, where snow cover was almost undetectable (Fig. 2), the residuals are relatively high—even above −0.6 mm—which is partially related to the sparseness of station observations and complex terrain conditions. The influence of effGS errors on snow depth estimation is examined in Section IV-D.

IV. Discussion

A. Role of the Predictor Variables in Simulating the Effective Grain Size

In the GlobSnow methodology, the effGS is defined as an effective value that can be iteratively optimized by mimicking

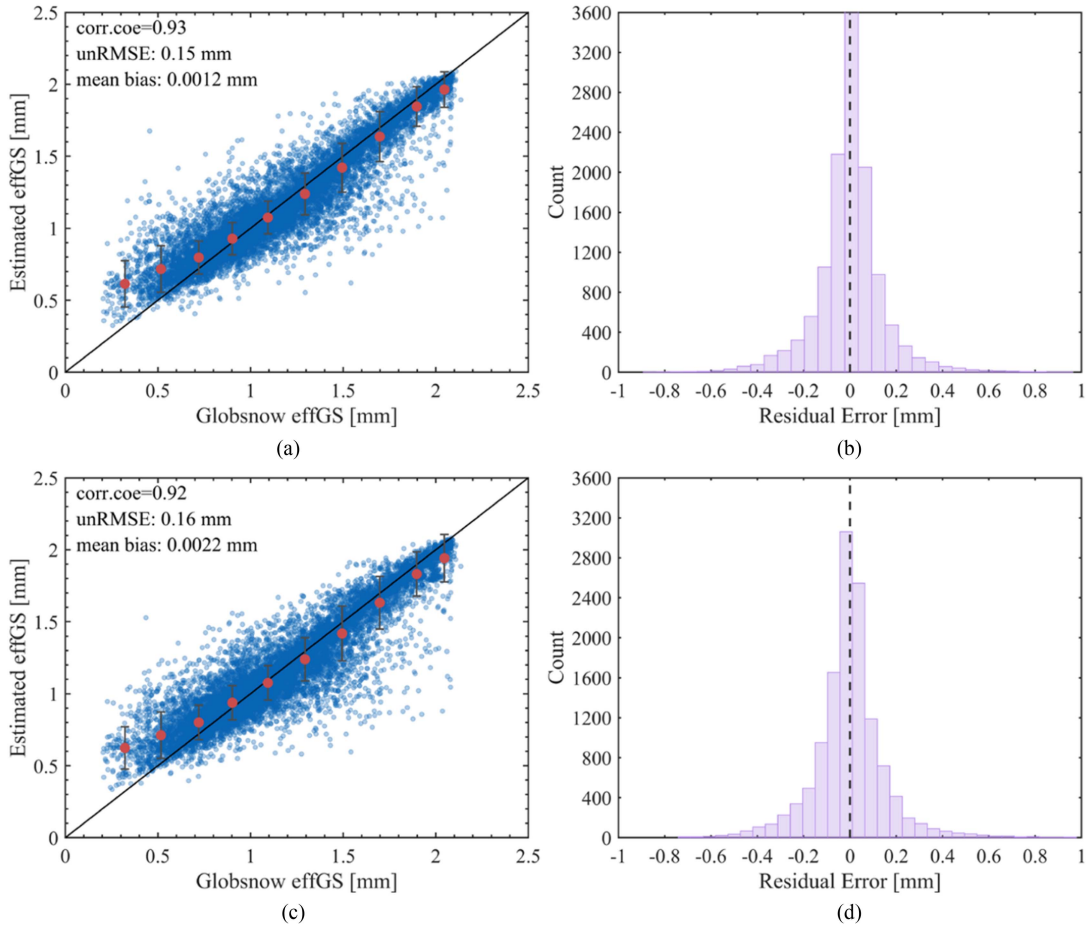

Fig. 13. Validation and comparison of the trained (a) RF_{withSD} and (c) $RF_{withoutSD}$ models over Eurasia. (b) and (d) Residual histograms for (a) and (c), respectively.

HUT modeling results and satellite observations. Typically, the microwave brightness temperature is affected not only by the SWE but also by multiple snow properties and states, such as snow stratigraphy, microstructure, and humidity [17], [18], [44], [45]. Moreover, forest cover generally complicates effGS retrieval, as attenuation due to the forest canopy quickly dominates the emission signal [46], [47]. Moreover, the homogeneous snowpack (single-layer) HUT model ignores complex layered structures and their interactions, resulting in high uncertainties in forward modeling [48], [49]. Therefore, effGS differs from the actual geometrical particle size. In addition, the autocorrelation among various variables reduces the role of the brightness temperature in predicting the effGS (Fig. 4).

Owing in part to these factors, the sensitivity of the brightness temperature to the effGS is low [Fig. 6(c) and (d)]. A signal with a high frequency, e.g., 89 GHz, is generally considered sensitive to surface snow particles [49], [50]. Fig. 6(d) indicates that the brightness temperature at 89 GHz decreased with increasing effGS within the 0.2–1.2 mm range. This occurs because the attenuation effect increasingly dominates with increasing volume scattering [9], [10], [18], [48], [49]. However, the brightness temperature at 89 GHz increased with the abundance of coarse-grained snow (typical size of 1.2–2.4 mm) because the penetration depth at 89 GHz is low and surface scattering of snowpacks dominates signal emission [12], [31], [33], [50]. The signals at 10.65 GHz exhibited less extinction than those at high frequencies (e.g., 36.5 GHz), penetrating almost the entire dry snowpack [48], [51]. Therefore, the signal could be considered more sensitive to the underlying soil properties, exhibiting a small response to the effGS [Fig. 6(d)]. At 18.7 GHz, the signals are affected by the soil and snow simultaneously, based on specific physical snowpack variables [48], [51].

For natural snow, the stratigraphic grain size typically increases from the top to the bottom layers, e.g., depth hoars in the bottom layers and rounded or faceted grains in the upper layers [10], [16]. However, the effGS represents a vertically averaged value because the snowpack is treated as a homogeneous single-layer medium in GlobSnow. Thus, the effGS exhibited a decreasing trend under shallow to moderate snow (0–60 cm) conditions [Fig. 6(a)]. However, under deep snow (60–120 cm) conditions, the effGS exhibited an increasing trend. This largely occurs because deep snow usually occurs during the middle to late snow season based on snowfall and accumulation patterns, and snow metamorphism significantly varies during this period, resulting in an upward trend in the effGS [26], [45], [48]. For snow depths greater than 120 cm, the effGS exhibited no change [Fig. 6(a)], mainly due to the signal saturation effects at 18.7 and 36.5 GHz under extremely deep snowpack conditions [48].

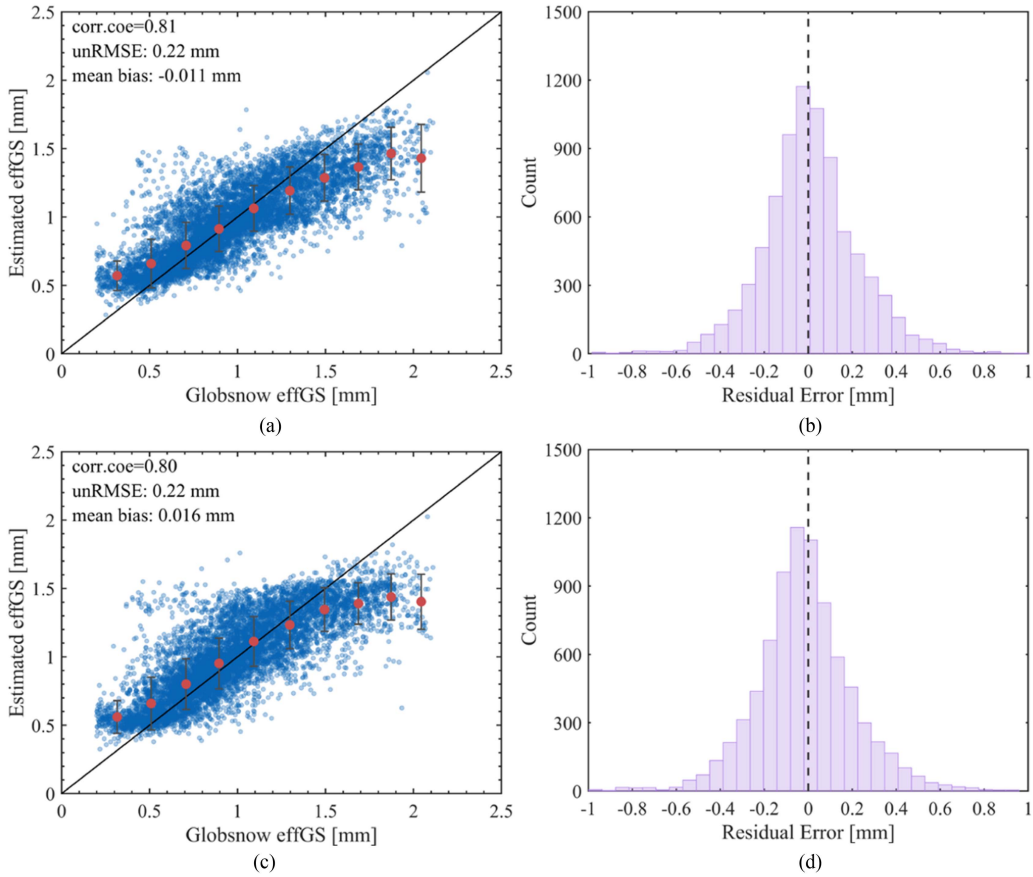

Fig. 14. Validation and comparison of the trained (a) $\mathrm{RF}_{\mathrm{withSD}}$ and (c) $\mathrm{RF}_{\mathrm{withoutSD}}$ models over North America. (b) and (d) Residual histograms for (a) and (c), respectively.

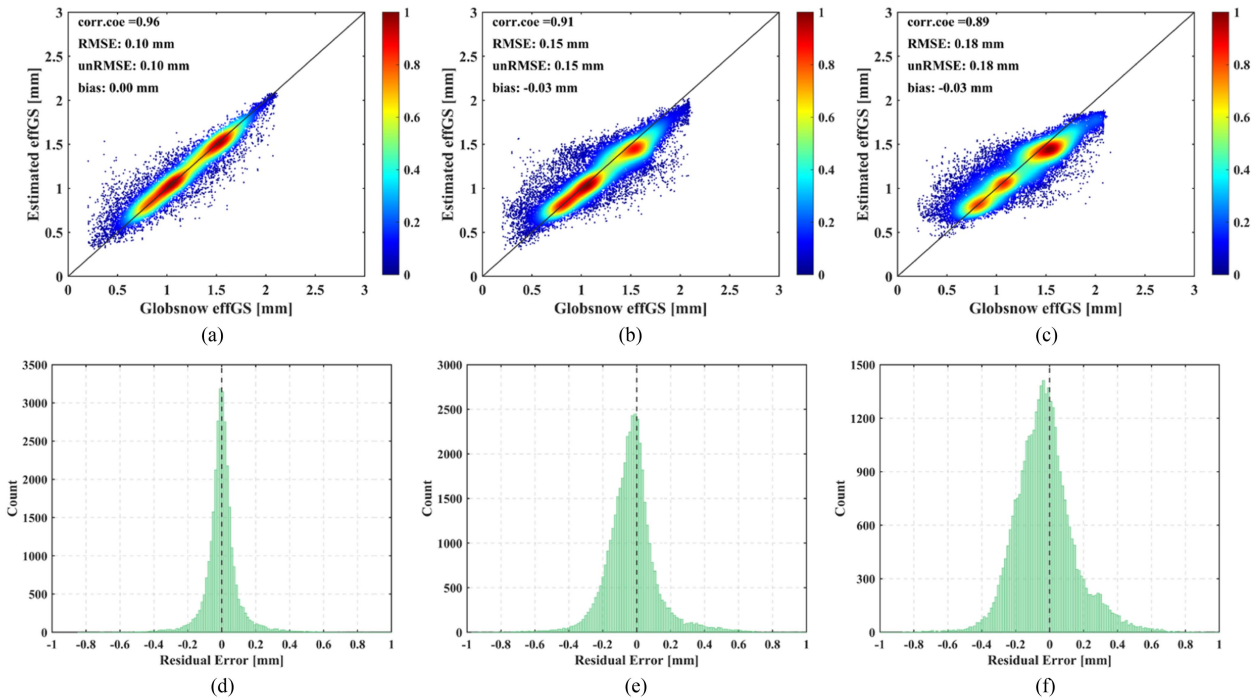

Fig. 15. Density scatterplots and histograms of the (a), (d) sample-based, (b), (e) temporal-based, and (c), (f) spatial-based 10-CV results for the RF model over Eurasia.

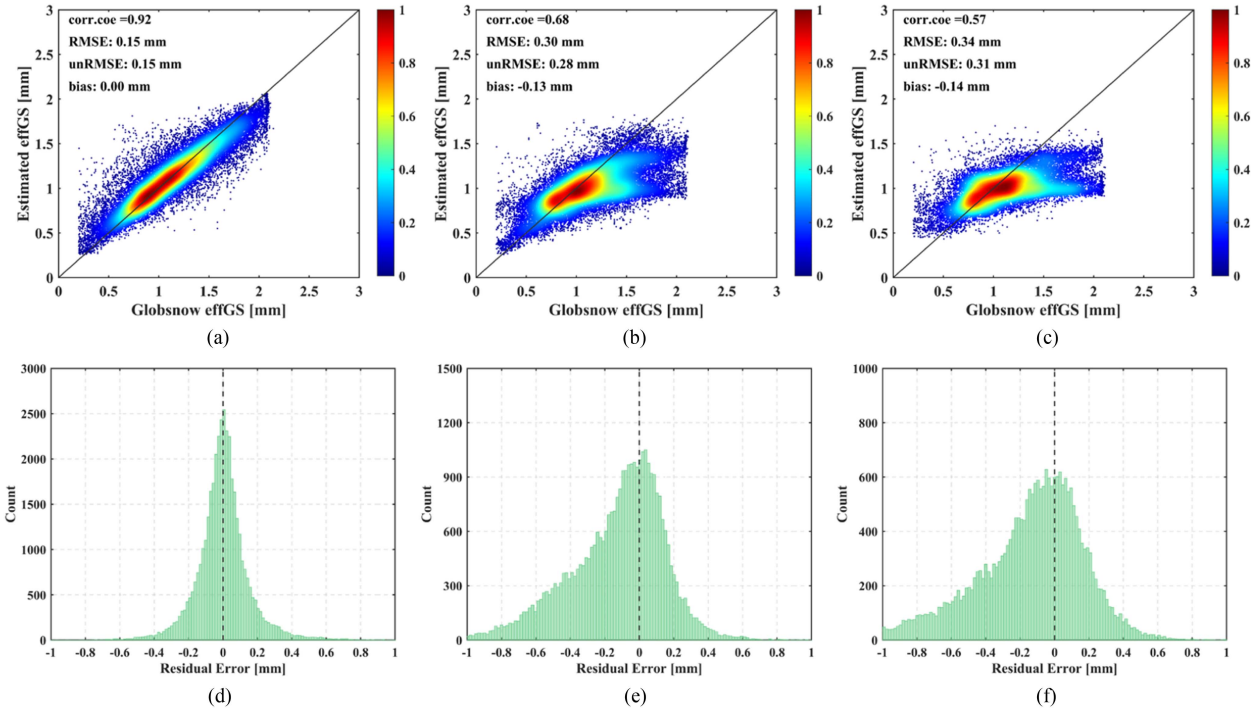

Fig. 16. Density scatterplots and histograms of the (a), (d) sample-based, (b), (e) temporal-based, and (c), (f) spatial-based 10-CV results for the RF model over North Ame.

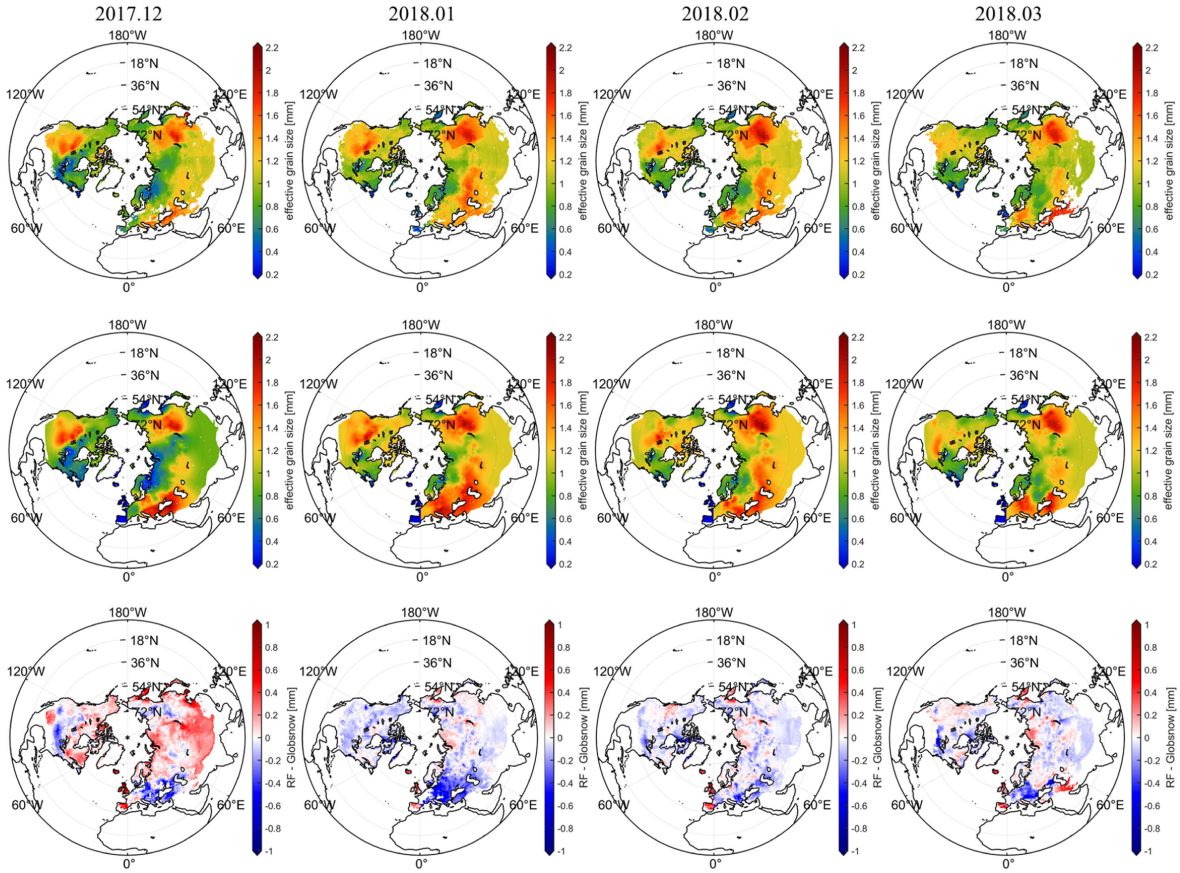

Fig. 17. Spatial distribution and comparison of the RF model estimates (top row) and GlobSnow (middle row) data and their differences (bottom row) during the snowy winter season in the Northern Hemisphere.

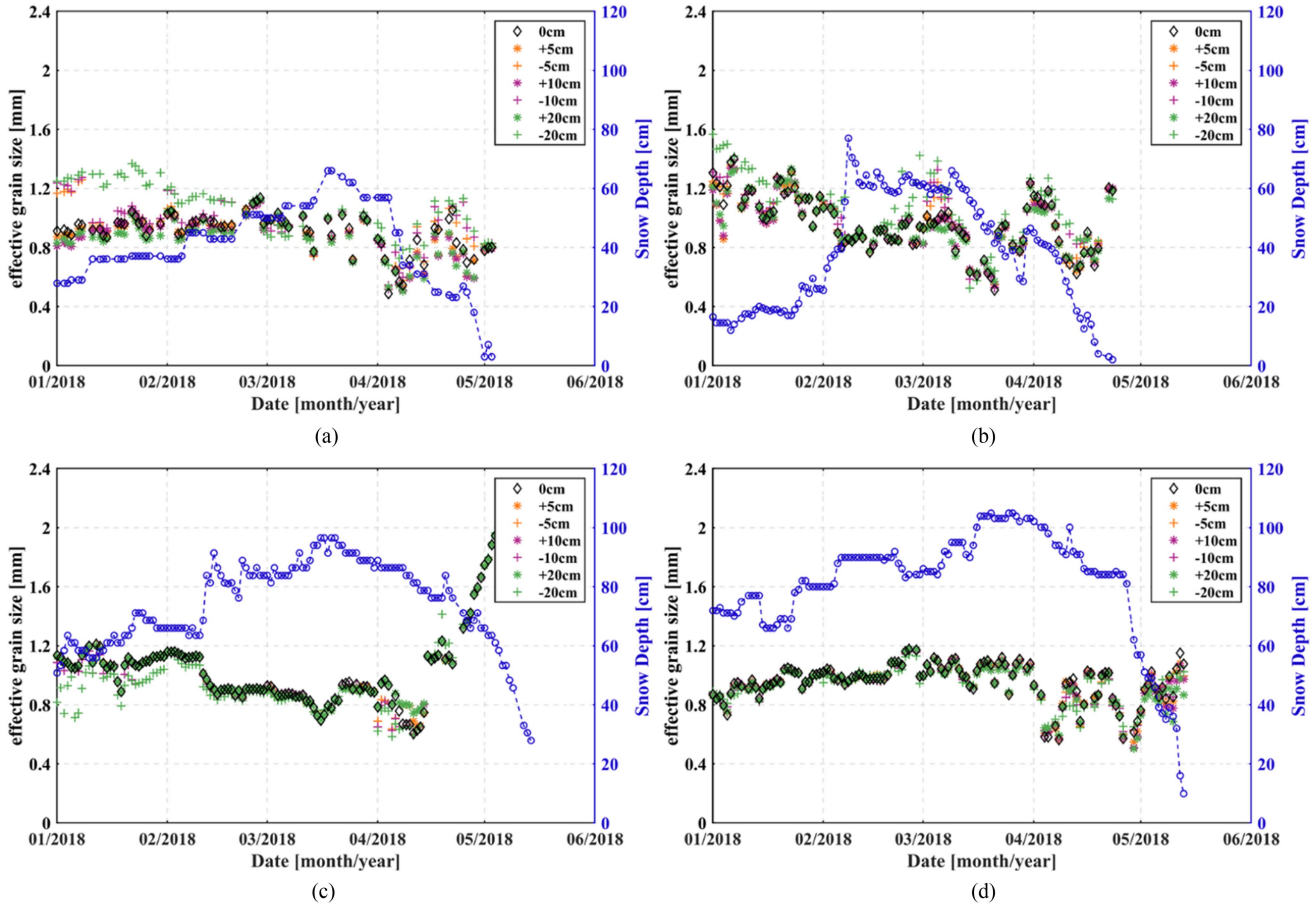

Fig. 18. Sensitivity of the effective grain size to snow depth priors in the four selected satellite pixels. (a) 62.39°N, 60.90°E. (b) 54.02°N, 122.78°W. (c) 63.31°N, 147.53°W. (d) 64.25°N, 60.95°E.

In GlobSnow, daily station-based effGS values were interpolated to a global spatial coverage by ordinary kriging interpolation; thus, the effGS exhibited notable spatial and temporal correlations with geographic elements and seasonal features, such as elevation, latitude, longitude, and DOY (Fig. 6). This is another reason that geographic elements and seasonal features are the most important predictor variables (Fig. 4), while snow depth priors do not notably improve effGS estimation (Figs. 8 and 9).

B. Transferability of the RF Models at Temporal and Spatial Scales

One possible question of data-derived machine learning techniques is their transferability on temporal and spatial scales [52], [53], [54]. The 10-CV results depicted in Figs. 15 and 16 demonstrate that the spatial predictions of the RF models exhibited greater uncertainties than did the temporal predictions. In contrast to the many stationary elements in the Earth system, e.g., soil types and soil properties, the snowpack is rapidly changing. Generally, the snow depth increases at the beginning of winter and then decreases in spring due to melting [22]; the grain size exhibits seasonal evolution [42] and a layered structure [48], [55]. Moreover, different spatial patterns of snow cover, such as generally deep snow in high-latitude and high-elevation areas, occur in various regions. Thus, rapid changes in snow characteristics limit the transferability of RF models to other areas.

In this study, the RF models performed better over Eurasia than over North America, for example, with unRMSE values of 0.18 and 0.31 mm, respectively, based on spatial analysis. One reason is that the terrain conditions over North America are complex, e.g., the Canadian Rocky Mountains, Coastal Mountains, San Juan Mountains, and the Appalachian Mountains. Fig. 6(b) shows that the elevation primarily contributed to predicting the effGS in low-elevation areas (below 1000 m). Moreover, the snow grain size generally varies significantly in mountainous areas due to the complex atmospheric circulation patterns there [56]. Additionally, the landscape in snow-covered areas of North America mainly comprises forest [see Fig. 1(b)], which dominates microwave radiation and complicates the relationship between the effGS and brightness temperature [22], [42].

The sample-based 10-CV method achieved the best performance among the three methods investigated (Figs. 15 and 16). This was likely because the spatially continuous effGS in GlobSnow was interpolated by ordinary kriging using daily station-based effGS values [22], causing the effGS to exhibit notable spatial and temporal correlations with elevation, latitude, longitude and DOY (Fig. 4). In this study, we applied temporal- and spatial-based 10-CV techniques to remove the effects of

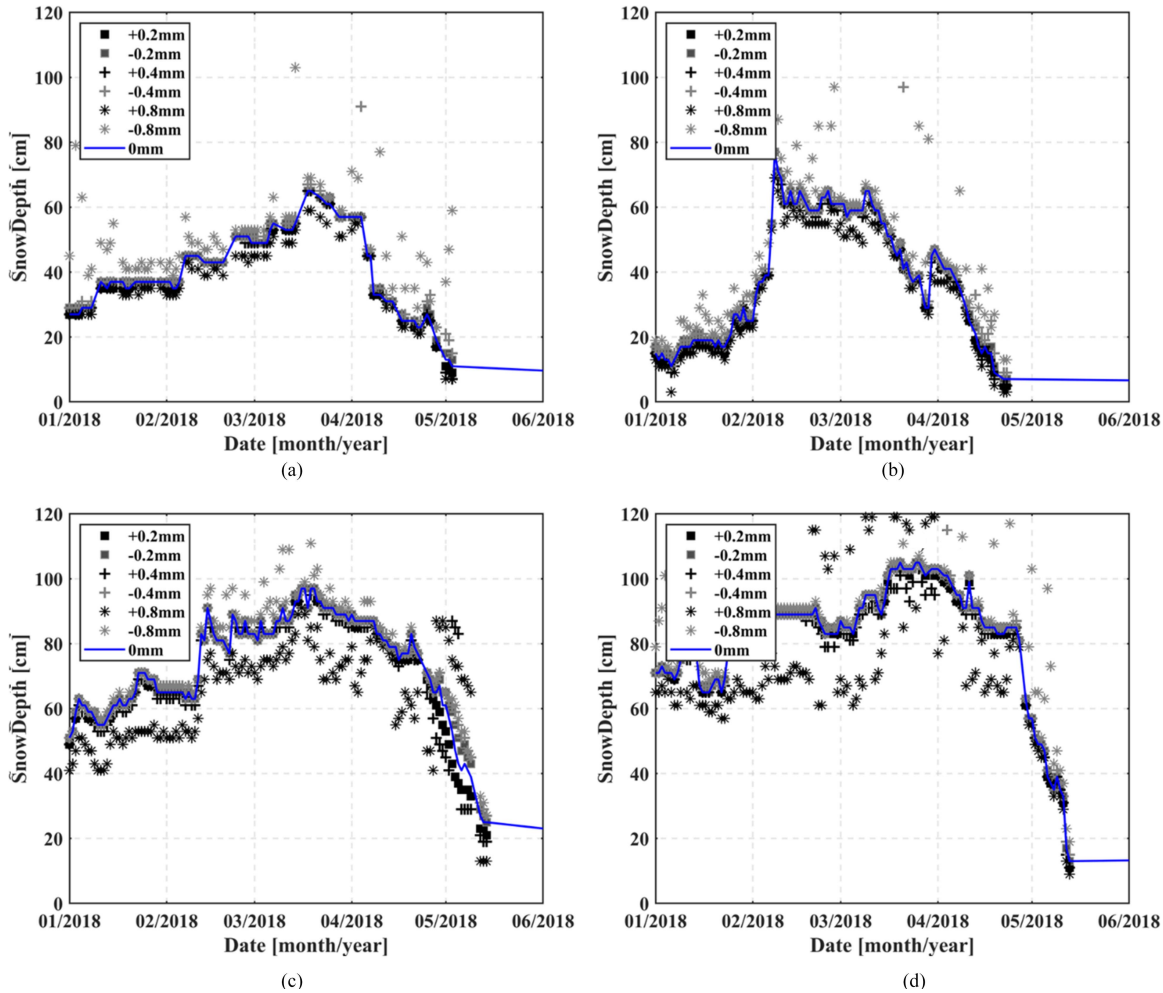

Fig. 19. Sensitivity of the snow depth optimized by the HUT model to biases from the effective grain size in the four selected satellite pixels. (a) 62.39°N, 60.90°E. (b) 54.02°N, 122.78°W. (c) 63.31°N, 147.53°W. (d) 64.25°N, 60.95°E.

spatial and temporal autocorrelations, providing a systematic and objective assessment of RF models for predicting the effGS.

C. Uncertainties in the Effective Grain Size Associated With Snow Depth

Neither gridded product nor station observations can provide true snow depth values; thus, the uncertainty in snow depth priors will propagate into the estimated effGS. Here, four satellite pixels located in North America and Eurasia were selected as examples. The RF model (RF_{withSD}), as described in Section II-C, was employed to simulate effGS values under the condition of adding biases ranging from ± 5 to ± 20 to the snow depth priors. Here, the highest bias was set to 20 cm according to the validation results in Fig. 5. Fig. 18 shows the sensitivity of the effGS to snow depth. The blue dashed line denotes the time series of snow depth recorded at stations. The asterisk ($*$) and plus ($+$) symbols denote the simulated effGS values after adding positive biases (5, 10, and 20 cm) and negative biases (-5, -10, and -20 cm), respectively, to the snow depth priors. The gray diamond ($\diamond$) denotes the effGS values simulated without adding any bias (0 cm) to the snow depth priors. The results indicate that the uncertainties in the effGS under shallow to moderate snow conditions (0–40 cm) are greater than those under deep snow conditions [Fig. 18(a) and (b) versus (c) and (d)]. Moreover, the underestimation of snow depth priors, namely, negative biases (e.g., -10 and -20 cm), generally results in high uncertainties in the effGS estimates, especially under shallow snowpack conditions. This occurs because the effGS exhibits a decreasing trend within the snow depth range of [0, 60] cm [Fig. 6(a)]. Thus, underestimation of the snow depth could cause an increase in the effGS [Fig. 18(a) and (b)]. For deep snowpacks (80 cm or deeper), the biases of the snow depth priors minimally influence the effGS estimates [Fig. 18(d)]. This occurs because the effGS for single-layer snow under deep snow conditions generally remains stable. Another reason is the signal saturation effects at 18.7 and 36.5 GHz under extremely deep snowpack conditions, which result in saturated satellite-observed brightness temperatures. Overall, the sensitivity of the effGS to snow depth priors is low for deep snow but relatively high for shallow snow. In particular, underestimation of either the ERA5-land product or station-based observations could cause high uncertainties in the effGS estimates; for example, the estimated effGS ranged from 0.8 to 1.2 mm at a bias of -20 cm [Fig. 18(a)]. Therefore, we

suggest that snow depth should be included in the RF model to predict effGS if sufficiently accurate prior information is available.

D. Uncertainties in the Assimilated Snow Depth Associated With the Effective Grain Size

According to the validation results in Section III, the effGS estimates of the RF model exhibited overestimation under low effGS conditions and underestimation under high effGS conditions, which could result in uncertainties in the snow depth estimates optimized by the HUT model [22], [26], [45]. Here, we applied the HUT model to optimize snow depth estimates by using a Bayesian assimilation method for four selected satellite pixels (Fig. 19). The overall unRMSE ranged from 0.15–0.31 mm (Figs. 13–16), and the maximum unRMSE reached 0.80 mm (Figs. 15 and 16); thus, the biases added to the effGS ranged from −0.8 to 0.8 mm, with a step of 0.2 mm. The blue solid line denotes the optimized snow depth without adding bias (0 cm) to the effGS. The different light-colored markers (■, +, and ∗) denote the optimized snow depth when negative biases (−0.2 to −0.8 mm) are added to the effGS, and the black markers (■, +, and ∗) denote the results when positive biases are added (0.2–0.8 mm). Overall, a positive effGS bias is more likely to cause uncertainties in the assimilated snow depth than a negative effGS bias, especially under deep snow conditions [Fig. 19(c) and (d)]. Notably, overestimation of the effGS typically results in a decreasing snow depth, whereas underestimation of the effGS results in an increasing snow depth, which is consistent with the results in Fig. 18. Fig. 19 also shows that the greater the biases are, the greater the uncertainties in the assimilated snow depth; for example, the differences in the assimilated snow depth could reach 30 cm after adding a 0.8 mm bias [Fig. 19(d)]. Moreover, we found that the assimilated snow depth under deep snow conditions is susceptible to effGS errors [Fig. 19(a) and (b) versus (c) and (d)]. Thus, reliable effGS priors are crucial for estimating snow depth with data assimilation methods [22].

V. Conclusion

The inclusion of prior snow information in the GlobSnow methodology undeniably reduces the uncertainties arising from snow metamorphism. However, the reliance on ground-based measurements is a severe limitation in areas where such information is unavailable. Furthermore, the GlobSnow methodology is computationally expensive when applied at the satellite scale. In this study, a new method was proposed to predict the effGS using a machine learning approach in which snow depth priors are not used. Our results highlighted the ability of the applied RF model to map the effGS from geolocation, terrain, seasonal characteristics, and spaceborne observations. The key conclusions are as follows.

1) Geographic location (latitude and longitude), terrain (elevation) and seasonal (DOY) characteristics primarily explain the variance in and patterns of the effGS.
2) Snow depth priors from ground-based measurements or gridded products are not necessary for predicting the effGS.
3) The application of spatially independent verification and the 10-CV method revealed that the effGS estimates favorably agreed with the GlobSnow reference data over Eurasia, with unRMSE values of 0.15–0.18 mm, but indicated a relatively high error over North America due to the terrain variability and heterogeneous forest cover, with overall unRMSE values of 0.22–0.31 mm.
4) The predicted effGS is susceptible to uncertainties in snow depth priors under shallow snow conditions. Errors in the predicted effGS could result in uncertainties in the assimilated snow depth under deep snow conditions. Thus, we suggest that snow depth priors should not be included in the RF model because sufficiently accurate data are lacking.

We are now attempting to produce an effGS time-series dataset by using the RF model and to optimize SWE retrieval via Bayesian nonlinear assimilation by leveraging RF- and GlobSnow-based effGS values. In future work, we will also compare SWE retrieval results and provide a comprehensive assessment of the SWE dataset in the Northern Hemisphere.

References

[1] T. Barnett, J. Adam, and D. Lettenmaier, "Potential impacts of a warming climate on water availability in snow-dominated regions," *Nature*, vol. 438, pp. 303–309, 2005, doi: 10.1038/nature04141.
[2] X. Qu and A. Hall, "On the persistent spread in snow-albedo feedback," *Climate Dyn.*, vol. 42, pp. 69–81, 2014, doi: 10.1007/s00382-013-1774-0.
[3] J. Mankin, D. Viviroli, D. Singh, A. Hoekstra, and N. Diffenbaugh, "The potential for snow to supply human water demand in the present and future," *Environ. Res. Lett.*, vol. 10, 2015, Art. no. 114016, doi: 10.1088/1748-9326/10/11/114016.
[4] J. Pulliainen et al., "Patterns and trends of Northern Hemisphere snow mass from 1980 to 2018," *Nature*, vol. 581, pp. 294–298, 2020.
[5] Y. Qin et al., "Agricultural risks from changing snowmelt," *Nature Climate Change*, vol. 10, pp. 459–465, 2020, doi: 10.1038/s41558-020-0746-8.
[6] A. Rango, A. Chang, and J. Foster, "The utilization of spaceborne microwave radiometers for monitoring snowpack properties," *Hydrol. Res.*, vol. 10, pp. 25–40, 1979.
[7] A. Chang, J. Foster, and D. Hall, "Nimbus-7 SMMR derived global snow cover parameters," *Ann. Glaciol.*, vol. 9, pp. 39–44, 1987.
[8] J. Pulliainen, "Mapping of snow water equivalent and snow depth in boreal and sub-arctic zones by assimilating space-borne microwave radiometer data and ground-based observations," *Remote Sens. Environ.*, vol. 101, pp. 257–269, 2006.
[9] L. Tsang et al., "Review article: Global monitoring of snow water equivalent using high-frequency radar remote sensing," *Cryosphere*, vol. 16, pp. 3531–3573, 2022, doi: 10.5194/tc-16-3531-2022.
[10] R. Kelly, A. Chang, T. Leung, and L. Foster, "A prototype AMSR-E global snow area and snow depth algorithm," *IEEE Trans. Geosci. Remote Sens.*, vol. 41, no. 2, pp. 230–242, Feb. 2003.
[11] R. Kelly, "The AMSR-E snow depth algorithm: Description and initial results," *J. Remote Sens. Soc. Jpn.*, vol. 29, pp. 307–317, 2009.
[12] L. Jiang, P. Wang, L. Zhang, H. Yang, and J. Yang, "Improvement of snow depth retrieval for FY3B-MWRI in China," *Sci. China Earth Sci.*, vol. 44, pp. 531–547, 2014.
[13] J. Wang, X. Huang, Y. Wang, and T. Liang, "Retrieving snow depth information from AMSR2 data for Qinghai–Tibet plateau," *IEEE J. Sel. Topics Appl. Earth Observ. Remote Sens.*, vol. 13, pp. 752–768, 2020, doi: 10.1109/JSTARS.2020.2970738.
[14] Y. Wei et al., "A dynamic snow depth inversion algorithm derived from AMSR2 passive microwave brightness temperature data and snow characteristics in Northeast China," *IEEE J. Sel. Topics Appl. Earth Observ. Remote Sens.*, vol. 14, pp. 5123–5136, 2021, doi: 10.1109/JSTARS.2021.3079703.

[15] R. Zhang et al., "Evaluation and adjustment of the AMSR2 snow depth algorithm for the Northern Xinjiang region, China," *IEEE J. Sel. Topics Appl. Earth Observ. Remote Sens.*, vol. 10, no. 9, pp. 3892–3903, Sep. 2017, doi: 10.1109/JSTARS.2016.2620521.
[16] M. Sturm and C. Benson, "Scales of spatial heterogeneity for perennial and seasonal snow layers," *Ann. Glaciol.*, vol. 38, pp. 253–260, 2004.
[17] I. Davenport, M. Sandells, and R. Gurney, "The effects of variation in snow properties on passive microwave snow mass estimation," *Remote Sens. Environ.*, no. 118, pp. 168–175, 2012.
[18] M. Durand and D. Liu, "The need for prior information in characterizing snow water equivalent from microwave brightness temperatures," *Remote Sens. Environ.*, vol. 126, pp. 248–257, 2012, doi: 10.1016/j.rse.2011.10.015.
[19] B. V. Jagt, M. Durand, S. Margulis, E. Kim, and N. Molotch, "The effect of spatial variability on the sensitivity of passive microwave measurements to snow water equivalent," *Remote Sens. Environ.*, vol. 136, pp. 163–179, 2013.
[20] I. Merkouriadi, J. Lemmetyinen, G. Liston, and J. Pulliainen, "Solving challenges of assimilating microwave remote sensing signatures with a physical model to estimate snow water equivalent," *Water Resour. Res.*, vol. 57, 2021, Art. no. e2021WR030119, doi: 10.1029/2021WR030119.
[21] L. Jiang, J. Shi, S. Tjuatja, J. Dozier, K. Chen, and L. Zhang, "A parameterized multiple-scattering model for microwave emission from dry snow," *Remote Sens. Environ.*, vol. 111, pp. 357–366, 2007.
[22] M. Takala et al., "Estimating northern hemisphere snow water equivalent for climate research through assimilation of space-borne radiometer data and ground-based measurements," *Remote Sens. Environ.*, vol. 115, pp. 3517–3529, 2011.
[23] L. Dai, T. Che, J. Wang, and P. Zhang, "Snow depth and snow water equivalent estimation from AMSR-E data based on a priori snow characteristics in Xinjiang, China," *Remote Sens. Environ.*, vol. 127, pp. 14–29, 2012.
[24] T. Che, L. Dai, X. Zheng, X. Li, and K. Zhao, "Estimation of snow depth from passive microwave brightness temperature data in forest regions of northeast China," *Remote Sens. Environ.*, vol. 183, pp. 334–349, 2016.
[25] J. Pan, M. Durand, M. Sandells, B. Vander Jagt, and D. Liu, "Application of a Markov Chain Monte Carlo algorithm for snow water equivalent retrieval from passive microwave measurements," *Remote Sens. Environ.*, vol. 192, pp. 150–165, 2017.
[26] J. Yang, L. Jiang, J. Lemmetyinen, J. Pan, K. Luojus, and M. Takala, "Improving snow depth estimation by coupling HUT-optimized effective snow grain size parameters with the random forest approach," *Remote Sens. Environ.*, vol. 264, 2021, Art. no. 112630.
[27] S. Hancock, R. Baxter, J. Evans, and B. Huntley, "Evaluating global snow water equivalent products for testing land surface models," *Remote Sens. Environ.*, vol. 128, pp. 107–117, 2013.
[28] J. Ahmad, B. Forman, E. Bair, and S. V. Kumar, "Passive microwave brightness temperature assimilation to improve snow mass estimation across complex terrain in Pakistan, Afghanistan, and Tajikistan," *IEEE J. Sel. Topics Appl. Earth Observ. Remote Sens.*, vol. 14, pp. 8849–8863, 2021, doi: 10.1109/JSTARS.2021.3102965.
[29] F. Larue, A. Royer, D. DeSève, A. Langlois, A. Roy, and L. Brucker, "Validation of GlobSnow-2 snow water equivalent over Eastern Canada," *Remote Sens. Environ.*, vol. 194, pp. 264–277, 2017.
[30] C. Mortimer et al., "Evaluation of long-term Northern Hemisphere snow water equivalent products," *Cryosphere*, vol. 14, pp. 1579–1594, 2020, doi: 10.5194/tc-14-1579-2020.
[31] L. Zschenderlein, K. Luojus, M. Takala, P. Venäläinen, and J. Pulliainen, "Evaluation of passive microwave dry snow detection algorithms and application to SWE retrieval during seasonal snow accumulation," *Remote Sens. Environ.*, vol. 288, 2023, Art. no. 113476.
[32] J. Herbert, M. Raleigh, and E. Small, "Reanalyzing the spatial representativeness of snow depth at automated monitoring stations using airborne Lidar data," *Cryosphere*, vol. 18, pp. 3495–3512, 2024, doi: 10.5194/tc-18-3495-2024.
[33] M. Tedesco and J. Jeyaratnam, "A new operational snow retrieval algorithm applied to historical AMSR-E brightness temperatures," *Remote Sens.*, vol. 8, 2016, Art. no. 1037.
[34] E. Bair, A. Abreu Calfa, K. Rittger, and J. Dozier, "Using machine learning for real-time estimates of snow water equivalent in the watersheds of Afghanistan," *Cryosphere*, vol. 12, pp. 1579–1594, 2018.
[35] X. Xiao, T. Zhang, X. Zhong, W. Shao, and X. Li, "Support vector regression snow-depth retrieval algorithm using passive microwave remote sensing data," *Remote Sens. Environ.*, vol. 210, pp. 48–64, 2018.
[36] E. Santi et al., "Exploiting the ANN potential in estimating snow depth and snow water equivalent from the airborne SnowSAR data at X- and Ku-bands," *IEEE Trans. Geosci. Remote Sens.*, vol. 60, 2021, Art. no. 4301216.
[37] X. Xu, X. Liu, X. Li, Q. Shi, Y. Chen, and B. Ai, "Global snow depth retrieval from passive microwave brightness temperature with machine learning approach," *IEEE Trans. Geosci. Remote Sens.*, vol. 60, 2022, Art. no. 4302917.
[38] S. Tanniru and R. Ramsankaran, "Machine learning-based estimation of high-resolution snow depth in Alaska using passive microwave remote sensing data," *IEEE J. Sel. Topics Appl. Earth Observ. Remote Sens.*, vol. 16, pp. 6007–6025, 2023, doi: 10.1109/JSTARS.2023.3287410.
[39] J. Pan et al., "Combination of snow process model priors and site representativeness evaluation to improve the global SnowDepth retrieval based on passive microwaves," *IEEE Trans. Geosci. Remote Sens.*, vol. 61, 2023, Art. no. 4301120, doi: 10.1109/TGRS.2023.3276651.
[40] K. Luojus et al., "GlobSnow v3.0 Northern Hemisphere snow water equivalent dataset," *Sci. Data*, vol. 8, 2021, Art. no. 163.
[41] K. Kouki, K. Luojus, and A. Riihelä, "Evaluation of snow cover properties in ERA5 and ERA5-land with several satellite-based datasets in the Northern Hemisphere in spring 1982–2018," *Cryosphere*, vol. 17, pp. 5007–5026, 2023, doi: 10.5194/tc-17-5007-2023.
[42] J. Rodriguez, A. Perez, and J. Lozano, "Sensitivity analysis of k-fold cross validation in prediction error estimation," *IEEE Trans. Pattern Anal. Mach. Intell.*, vol. 32, no. 3, pp. 569–575, Mar. 2010.
[43] J. Pulliainen and M. Hallikainen, "Retrieval of regional snow water equivalent from spaceborne passive microwave observations," *Remote Sens. Environ.*, vol. 75, pp. 76–85, 2001.
[44] M. Sturm, J. Holmgren, and G. E. Liston, "A seasonal snow cover classification system for local to global applications," *J. Climate*, vol. 8, pp. 1261–1283, 1995.
[45] A. Kontu, J. Lemmetyinen, J. Vehviläinen, L. Leppänen, and J. Pulliainen, "Coupling SNOWPACK-modeled grain size parameters with the HUT snow emission model," *Remote Sens. Environ.*, vol. 194, pp. 33–47, 2017.
[46] A. Roy, A. Royer, J. Wigneron, A. Langlois, J. Bergeron, and P. Cliche, "A simple parameterization for a boreal forest radiative transfer model at microwave frequencies," *Remote Sens. Environ.*, vol. 124, pp. 371–383, 2012.
[47] Q. Li et al., "The influence of thermal properties and canopy-intercepted snow on passive microwave transmissivity of a scots pine," *IEEE Trans. Geosci. Remote Sens.*, vol. 57, no. 8, pp. 5424–5433, Aug. 2019.
[48] J. Lemmetyinen et al., "Simulating seasonally and spatially varying snow cover brightness temperature using HUT snow emission model and retrieval of a microwave effective grain size," *Remote Sens. Environ.*, vol. 156, pp. 71–95, 2015.
[49] G. Picard, M. Sandells, and H. Löwe, "SMRT: An active-passive microwave radiative transfer model for snow with multiple microstructure and scattering formulations (v1.0)," *Geosci. Model Develop.*, vol. 11, pp. 2763–2788, 2018.
[50] G. Picard, F. Domine, G. Krinner, L. Arnaud, and E. Lefebvre, "Inhibition of the positive snow-albedo feedback by precipitation in interior Antarctica," *Nature Climate Change*, vol. 2, pp. 795–798, 2012, doi: 10.1038/nclimate1590.
[51] C. Derksen, "The contribution of AMSR-E 18.7 and 10.7 GHz measurements to improved boreal forest snow water equivalent retrievals," *Remote Sens. Environ.*, vol. 112, pp. 2701–2710, 2008.
[52] M. Reichstein, G. Camps-Valls, B. Stevens, M. Jung, J. Denzler, and N. Carvalhais, "Deep learning and process understanding for data-driven Earth system science," *Nature*, vol. 566, pp. 195–204, 2019.
[53] J. Yang et al., "Snow depth estimation and historical data reconstruction over China based on a random forest machine learning approach," *Cryosphere*, vol. 14, pp. 1763–1778, 2020, doi: 10.5194/tc-14-1763-2020.
[54] N. Kanda and C. Fletcher, "Evaluating a hierarchy of bias correction methods for ERA5-land SWE in northern Canada," *EGUsphere*, 2024, doi: 10.5194/egusphere-2024-639.
[55] J. Lemmetyinen et al., "A comparison of airborne microwave brightness temperatures and snowpack properties across the boreal forests of Finland and Western Canada," *IEEE Trans. Geosci. Remote Sens.*, vol. 47, no. 3, pp. 965–978, Mar. 2009.
[56] J. Dozier, E. Bair, and R. Davis, "Estimating the spatial distribution of snow water equivalent in the World's mountains," *WIREs Water*, vol. 3, pp. 461–474, 2016.

Jianwei Yang received the M.S. degree in geography from the University of Chinese Academy of Sciences, Beijing, China, in 2017, and the Ph.D. degree in geography from Beijing Normal University, Beijing, China, in 2021.

He is currently an Assistant Professor with the Faculty of Geographical Science, Beijing Normal University. His research interests include the interaction of microwaves with snowpacks, microwave remote sensing of the cryosphere, and the development of algorithms for snow parameters, e.g., snow depth, snow water equivalent, and snow density.

Lingmei Jiang (Member, IEEE) received the Ph.D. degree in geography from Beijing Normal University, Beijing, China, in 2005.

She is currently a Professor with the Faculty of Geographical Science, Beijing Normal University. She has authored or coauthored more than 150 scientific publications. Her research interests include microwave emission/scattering modeling of the land surface, passive microwave remote sensing of the snow water equivalent, soil moisture, and the surface freeze/thaw state.

Dr. Jiang was awarded the Shi Yafeng Prize for Young Scientists in Cryosphere and Environment in 2018.

Juha Lemmetyinen (Member, IEEE) received the D.Sc. (Tech.) degree in electrical engineering from Aalto University [formerly the Helsinki University of Technology (TKK)], Espoo, Finland, in 2012.

From 2004 to 2008, he was a Researcher with the Laboratory of Space Technology, Department of Radio Science and Engineering, TKK, where he specialized in radiometer calibration techniques and remote sensing. He has been with the Finnish Meteorological Institute, Helsinki, Finland, since 2009, leading the Cryosphere Processes Research Group since 2014. His research interests include the application of active and passive microwave instruments in the remote sensing of snow cover.

Kari Luojus received the M.Sc., Lic.Sc. (Tech.), and D.Sc. (Tech.) degrees in space technology from the Helsinki University of Technology (TKK), Espoo, Finland, in 2004, 2007, and 2009, respectively.

Since 2008, he has been a Research Scientist and Senior Research Scientist with the Arctic Research Department of the Finnish Meteorological Institute, Helsinki, Finland. He was a Project Manager for the ESA DUE GlobSnow project between 2008 and 2012, which focused on constructing long-term essential climate variables related to terrestrial snow cover. He was also a Project Manager for the ESA DUE GlobSnow-2 project (2012–2014). His research interests include the development of active and passive microwave remote sensing techniques for cryospheric and hydrological applications.

Dr. Luojus is a Steering Group Member for the WMO Global Cryosphere Watch and a Coleader for the WMO GCW Snow Watch Group.